Bull. Chem. Soc. Ethiop. **2026**, 40(7), 1569-1580.
DOI: https://dx.doi.org/10.4314/bcse.v40i7.14
ISSN 1011-3924
Printed in Ethiopia
Online ISSN 1726-801X
© 2025 Chemical Society of Ethiopia and The Authors

INVESTIGATION OF THE CORROSION RESISTANCE OF CHROMATE CONVERSION COATING ON ALUMINIUM IN 3% SODIUM CHLORIDE

G. Venkatesh[1], M. G. L. Annaamalai[2], A. Manikandan[3], D. Shanmugapriya[4], P. Vennila[5]

[1]Department of Biomaterials, Saveetha Dental College and Hospitals, SIMATS, Saveetha University, Chennai-600077, India
[2]Department of Civil Engineering, VSA Group of Institutions, Salem-636010, Tamil Nadu, India
[3]Centre for Material Chemistry, Department of Chemistry, Karpagam Academy of Higher Education, Coimbatore 641021, Tamil Nadu, India
[4]Vicerrectoría de Investigación y Postgrado, Universidad de La Serena, Chile. Código postal: 1700000
[5]Department of Chemistry, Thiruvalluvar Government Arts College- Rasipuram-Namakkal, Tamil Nadu, India- 637401

(Received June 16, 2025; Revised August 13, 2025; Accepted March 11, 2026)

ABSTRACT. Aluminum is an increasingly important material in the metals industry, ranking as one of the most abundant elements in the Earth's crust and one of the most widely used metals alongside steel. To prevent corrosion, protective conversion coatings are commonly applied through processes such as phosphating, chromating, or oxalating. This study investigates the porosity and adhesion of chromate conversion coatings on aluminum, evaluated using appropriate testing methods. The surface morphology and structure of the coatings were characterized by scanning electron microscopy (SEM). Corrosion resistance was assessed through Tafel polarization and electrochemical impedance spectroscopy (EIS). Furthermore, the thermodynamic properties of chromate-coated aluminum were examined. The effects of immersion time, temperature, and chromic acid concentration on coating performance were systematically studied; these parameters were found to enhance coating properties up to an optimal point, beyond which performance declined. SEM analysis further revealed variations in surface characteristics of the coating under different processing conditions.

KEY WORDS: Aluminium, Corrosion, Electrochemical analysis, Scanning electron microscopy, Thermodynamic parameters

INTRODUCTION

Electrochemical reactions involving metal surfaces, such as anodic dissolution and coupled reduction processes, result in the formation of protective conversion layers. Chromate conversion coatings have been widely used to enhance the corrosion resistance of metals and aluminum alloys in various manufactured products, including aircraft and automotive components [1-3]. The utilization of aluminum hinges on three primary characteristics: its lightweight nature, the mechanical strength achieved via suitable alloying and thermal treatment, and the inherent corrosion resistance of the pure metal [4]. The degradation of metals due to external influences, including alkalinity, high concentrations of aggressive chloride ions, the presence of cracks, and variations in layer thickness, significantly impacts the structural integrity of metal structures. Accordingly, it is imperative to implement corrosion prevention strategies that are effective in industrial applications [5]. Reducing energy losses through the development of new hole and electron acceptors and the optimization of charge transfer kinetics has been the focus of recent research. Controlling nanoscale morphology, along with interfacial engineering in device architectures, has also been a major focus to enhance efficiencies toward their theoretical limits.

*Corresponding author. E-mail: venkateshindhuja@gmail.com
This work is licensed under the Creative Commons Attribution 4.0 International License

Furthermore, numerous studies highlight that solid-state hole transport materials serve as promising substitutes for liquid electrolytes, which are often toxic, volatile, and corrosive to cell components [6]. Although innumerable corrosion control strategies have been proposed and tested, no single approach has been universally effective. Additionally, materials with exceptional thermal and electrical conductivity are particularly advantageous for applications in the food and chemical sectors [7-11]. Chromate conversion coatings are frequently applied to a variety of engineering substrates in order to enhance paint adhesion, achieve specific surface finishes, and improve corrosion resistance [12]. Aluminium is becoming an increasingly important part of the metals industry.

Chromate coatings form a key pretreatment for paint adhesion in paintwork and powder coating applications, while delivering robust corrosion protection [13-16]. Common applications include household appliances, coil coatings, aircraft, and electronic devices. These coatings are preferred over chromium phosphate because they have low contact resistance and allow for spot welding. Chromate coatings are highly effective corrosion inhibitors and widely used in manufacturing, transportation, defence, equipment, automotive, and bodywork. The use of conversion coating with hexavalent chromium has been a well-established technique for safeguarding aluminium alloys against corrosion, and it is effectively utilized on various metals and alloys [17-21]. Additionally, chromium-based paints find application on bridges and ships. Most military vehicles currently employ chromates to safeguard aluminium against corrosion. The literature indicates that chromates perform effectively in the salt spray test. Many government organizations are actively seeking alternative chromate-free systems that provide similar levels of protection and are prepared to conduct tests on these options.

Coatings research and development has normally concentrated on improving corrosion resistance and optimizing coating thickness. Some scientists have discovered that chromate-based coatings have a unique self-healing property. When a coated surface is scratched, chromate ions may flow laterally to the affected area and form a protective layer over the recently exposed metal. This migration prevents additional corrosion by shielding the bare surface. Chrome plating is probably the most common finish in the aerospace industry. Chromate conversion coatings are used on aluminium alloys to improve their corrosion resistance and paintability. Chromium is a metallic element that is both light and hard [22-28]. When used properly, chromium has excellent corrosion resistance, wear resistance, and strength. Chromium conversion coatings are typically thought of as a redox reaction involving chromate ions and the substrate metal.

In the present study, the porosity and adhesion of chromate-coated aluminium were determined using appropriate testing methods. A scanning electron microscope uses a focused beam of high-energy electrons to produce a variety of signals on the surface of solid specimens [29-32]. The signal resulting from electron-sample interaction, which includes the external morphology, chemical composition, crystalline structure, and orientation of the materials in the sample. In scanning mode, a conventional technique can be used to image a scanning area ranging in width from 1 cm to 5 microns. SEM analysis was used to investigate the coating's surface morphology and structure. We used Tafel polarization and impedance methods to investigate the corrosion behaviour of chromate-coated aluminium. Thermodynamic parameters for different batches of chromate-coated aluminium were also calculated.

EXPERIMENTAL

Preparation of samples

To achieve high-quality coatings with the desired physical and chemical properties, it is essential to properly prepare the baths and ensure the solution is free of metallic and other contaminants (Table 1). The water used to make the conversion coating bath was double-distilled and de-mineralized. All glassware was washed by soaking overnight in a 1:1 mixture of nitric acid and

sulfuric acid. After washing with tap water and distilled water, they were dried and used. The various bath compositions used in this study are given in Table 1 below. Then the pretreated aluminum samples were weighed (w_1) and immersed in the above-mentioned solutions of the chromate conversion coating for different periods of time, i.e., 2-10 minutes, and a temperature range of 30-50 °C. The samples were rinsed thoroughly with double-distilled water to remove any chloride ions from the tap water. They were then dried and weighed. The weight of the conversion coating formed on aluminium was calculated using the formula:

W = (W2-W1) g, where W1 is the weight before coating, and W2 is the weight after coating.

The thickness of the chromate conversion coating was calculated using the following equation

$$T = \frac{\mathrm{W\,X\,10000}}{\mathrm{A\,X\,d}}$$

where, T = thickness in microns, W = Weight of the coating in g, A = coated area in cm, d = density of aluminium.

The chromate conversion-coated aluminum plates were heat-treated by placing them in a closed oven at 300 °C for 4 hours. Then, the heat-treated samples were immediately placed in cold water and observed to see whether or not any surge was visually seen on the surface.

Table 1. Details of bath solution preparations.

S. No.	Sample	Percentage of chromic acid and sodium fluoride
1	Solution-I	Chromic acid – 3 % (v/v) and sodium fluoride - 0.3 % (v/v)
2	Solution-II	Chromic acid -5 % (v/v) and sodium fluoride - 0.3% (v/v)
3	Solution-III	Chromic acid - 7 % (v/v) and sodium fluoride - 0.3 % (v/v)

Corrosion studies

Tafel polarization studies

Tafel polarization is a highly effective technique for determining a specimen's corrosion resistance. Cathodic and anodic polarization curves were obtained potendiodynamically by immersing the chromate conversion-coated aluminium specimens, used as working electrodes, in a 3% sodium chloride solution using a computer-controlled Thales impedance analyzer. The counter electrode is platinum, while the reference electrode is calomel.

Electrochemical impedance studies

Electrochemical impedance spectroscopy (EIS) acts as a successful tool for assessing the corrosion behavior of materials. This study involved conducting AC impedance measurements utilizing a Thales impedance analyzer across a frequency spectrum of 10 mHz to 100 kHz, applying an AC perturbation amplitude of 10 mV on the open-circuit potential. The electrochemical cell configuration for EIS was the same as that used for the Tafel polarization measurements.

Scanning electron microscope analysis

SEM images were acquired using the JEOL-JSM-35 LF, which operates at an accelerating voltage range of 5-35 kV and offers magnification from 10 to 180,000 times. SEM images for the current studies were captured at 25 KV with a magnification of 1000x.

Thermodynamic parameters

The activation energy (E_a), which is the minimum energy required for the reaction to occur, can be calculated from the Arrhenius equation.

$$k = Ae^{-Ea/RT} \quad (1)$$

E_a is calculated from the slope of the plot log(k) vs 1/T as follows

$$\text{Slope} = -E_a / 2.303R \quad (2)$$

$$E_a = -(\text{slope X } 2.303R) \quad (3)$$

Enthalpy of activation is calculated from the slope of the plot of log(K/t) vs 1/t using the equation.

$$-\Delta H^\circ = \text{slope X } 2.303R \quad (4)$$

Entropy of activation is calculated from the intercept of the plot of log(K/t) vs 1/t using the equation.

$$\text{Log}(R/Nh) - \Delta S^\circ/2.303 = \text{intercept} \quad (5)$$

h= planck's constant ($6.625 \text{ X } 10^{-34}$)
R = Gas constant (8.314)
Free energy of activation is calculated from the following equation.

$$\Delta G^\circ = \Delta H^\circ - T\Delta S^\circ \quad (6)$$

RESULTS AND DISCUSSION

Effect of immersion time

Table 2 illustrates the effect of immersion duration at varying temperatures on the weight, thickness, and growth rate of the conversion coating on aluminium. As immersion duration increases, the coating weight and thickness initially ascend, reaching a maximum at approximately 6 minutes. Beyond this threshold, both weight and thickness begin to diminish. This reduction is attributed to the dissolution of aluminium during the coating process, where prolonged immersion results in excessive dissolution, leading to the formation of degraded deposits such as charred or powdery residues. These elements contribute to a decrease in both the deposit weight and the overall coating growth rate.

Table 2. Effect of immersion time on various properties of chromate conversion coating obtained from chromic acid Solutions I, II, and III at 30 °C, 40 °C, and 50 °C.

Time (Sec)	Temperature °C	Solution-I		Solution-II		Solution -III	
		Weight of coating (mg)	Thickness (μ)	Weight of coating (mg)	Thickness (μ)	Weight of coating (mg)	Thickness (μ)
120	30	0.5	0.06	0.4	0.05	0.3	0.04
240		1	0.14	1.1	0.15	0.9	0.12
360		1.4	0.19	1.7	0.23	1.2	0.16
480		0.7	0.09	0.9	0.12	0.6	0.08
600		0.5	0.06	0.6	0.08	0.4	0.05
120	40	0.4	0.05	0.3	0.04	0.2	0.03
240		0.8	0.11	0.9	0.12	0.7	0.09
360		1.1	0.15	1.4	0.19	0.9	0.12
480		0.5	0.07	0.6	0.08	0.3	0.04
600		0.2	0.03	0.3	0.04	0.2	0.03

120	50	0.3	0.04	0.2	0.03	0.1	0.01
240		0.5	0.07	0.6	0.08	0.4	0.05
360		0.9	0.12	1	0.14	0.8	0.11
480		0.4	0.05	0.5	0.07	0.2	0.03
600		0.1	0.01	0.2	0.03	0.1	0.01

Effect of immersion temperature

Figure 1 illustrates the influence of temperature on the thickness of the chromate conversion coating derived from different baths. It was found that as the temperature of the bath rose, the weight and thickness of the deposit diminished. The dissolution rate of aluminium surpasses the coating formation rate at elevated temperatures [33]. Table 3 illustrates the influence of chromic acid and sodium fluoride concentrations on the coating rate of aluminium at 30 °C, over a duration of 6 minutes. The tables demonstrate that an increase in chromic acid concentration markedly enhances the coating thickness, consequently augmenting the deposit thickness.

Thermodynamic parameters

To understand the thermodynamics of chromate conversion layer formation on aluminium, activation parameters such as E_a, ΔH°, ΔS°, and ΔG° were assessed. The computed thermodynamic parameters for the chromate coating on aluminium, derived from various solutions I-III at distinct temperatures, are presented in Table 3. The negative values of activation enthalpy (ΔH°) and free energy of activation (ΔG°) suggest that the chromate conversion reaction on aluminium is exothermic and thermodynamically favorable. A negative ΔH° implies that energy is released during the formation of the chromate layer, while a negative ΔG° confirms that the reaction proceeds spontaneously under the given conditions. Additionally, the positive value of activation entropy (ΔS°) indicates an increase in disorder, likely due to the release of water or other by-products during the surface reaction. Together, these parameters point toward a reaction mechanism that is energetically downhill and entropy-driven, possibly involving the adsorption of chromate ions followed by surface redox reactions, which facilitate the stable conversion coating on aluminium. Maximum attainable thickness with 0.5 percent CrO_3. Beyond this concentration, the thickness of the coating diminishes. This may result from heightened aluminium dissolution. CrO_3 is a highly aggressive electrolyte, and its aggressiveness, along with its dissolution, escalates with higher concentrations [34]. Consequently, layer formation diminishes with increasing CrO_3 concentration.

Table 3. Thermodynamic parameters for the chromate coating from various samples.

Samples	E_a	ΔH°	ΔS°	ΔG°	% CrO_3	30 °C	40 °C	50 °C
Solution-I	11.53	0.13	-23.80	-7449.67	0.3%	0.19	0.15	0.12
Solution-II	5.27	0.16	-23.78	-7445.08	0.5%	0.23	0.19	0.14
Solution-III	7.08	0.14	-23.79	-7447.61	0.7%	0.16	0.12	0.11

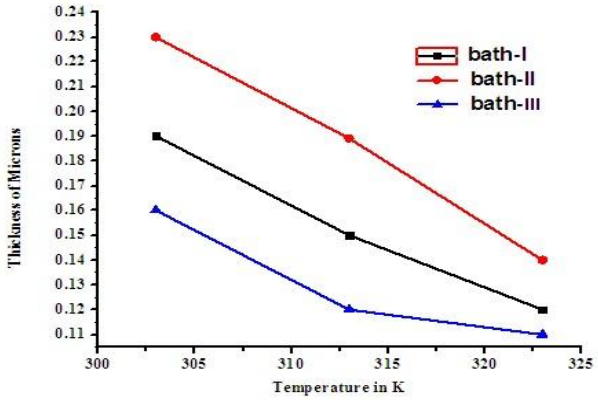


Figure 1. Effect of temperature on the thickness of chromate conversion coating for various solutions.

Effect of NaF

The incorporation of NaF into the chromate solution inhibits the excessive dissolution of Al chromate via complexation and facilitates its removal as AlF. The optimal concentration for observing increased coating thickness is 0.03 M NaF. At a concentration exceeding 0.03 M NaF, the thickness of the coating was diminished. This results from an augmented etching thickness associated with a higher concentration of fluoride ions, which more aggressively degrade the aluminium surface. This elevated etching inhibits the development of coatings. The thickness diminishes with increased NaF concentration.

Corrosion studies

Table 4 displays the weight loss and corrosion inhibition efficacy of chromate-coated aluminium in different solutions. The table indicates that post-immersion weight loss is more significant for uncoated aluminium compared to chromate-coated aluminium, and this loss diminishes as the thickness of the chromate coating increases. Aluminium treated with a solution of 0.5 percent CrO_3 and 0.03 percent NaF exhibits superior corrosion resistance compared to alternative plates. The inhibitory effect intensifies with rising concentrations of chromic acid until a specific threshold, beyond which it diminishes. This may be due to chloride ions exhibiting a diminished affinity for chromate-coated aluminium, as the chromate coating is robustly and intrinsically established on the aluminium surface [35, 36].

Table 4. Weight loss and inhibition efficiency of chromate-coated aluminium from various solutions.

S.No	Sample	Weight loss (g)	Inhibition efficiency (%)	Surface coverage (θ)
1	Uncoated Al	0.004	-	-
2	Chromate-coated Solution-I	0.0008	80	0.80
3	Chromate-coated Solution-II	0.0004	90	0.90
4	Chromate-coated Solution-III	0.0005	87	0.87

Potentiodynamic polarization studies

Corrosion potentials are generally in close proximity to open circuit potentials (OCP). The corrosion potential is markedly altered due to the surface modification from chromate coating and the adherence of certain corrosion products. Tangents were derived from OCP values within 100 mV, and the anodic and cathodic slopes of the plate were assessed after 168 hours of immersion in a 3% sodium chloride solution. Table 4 and Figure 2 illustrate that the cathodic slope (b_c) and anodic slope (b_a) of both coated and uncoated aluminium samples rise with greater deposit thickness. Table 4 indicates that the corrosion current and corrosion rate of aluminium samples coated with chromate were significantly lower than those of uncoated aluminium [37, 38]. The corrosion current and corrosion rate diminished with an increase in the thickness of the chromate coating [39]. The aluminium coated with solution-II exhibits the lowest corrosion current and rate, indicating that a chromate coating enhances aluminum's corrosion resistance, which improves with increased coating thickness. The elevated corrosion resistance values of the chromate-coated samples, along with impedance analyses and comparisons to solution-I and solution-III, further corroborate this finding. The inhibitory effect intensifies with rising concentrations of chromic acid until a specific threshold, beyond which it diminishes.

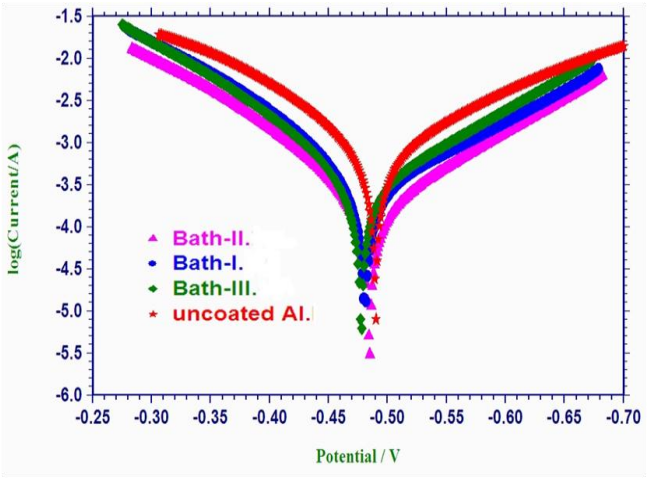


Figure 2. Comparison of Tafel plots for bare and chromate conversion-coated aluminium from solution- I, II, III.

Table 4. Corrosion parameters obtained from potentiodynamic polarizations and electrochemical impedance.

Substrate	E_{corr} (mV)	I_{corr} (μA)	IE (%)	R_{ct} (Ω.cm^2)	C_{dl} (μF/cm^2)	IE(%)
Bare Al	-0.490	8.774	-	24	919	-
Solution-I	-0.481	3.517	59	53	408	55
Solution-II	-0.485	1.889	78	89	247	73
Solution-III	-0.478	3.398	61	67	371	64

Electrochemical impedance spectroscopy studies

Figure 3 illustrates that aluminium coated with solution-II exhibits greater impedance than the other plates. The impedance escalates in direct correlation with the thickness of the chromate coating. Uncoated aluminium exhibits the lowest impedance among the three materials. Consequently, it can be inferred that chromate coatings markedly enhance corrosion resistance, with resistance improving as the thickness of the chromate coating increases. The SEM data confirms that aluminium coated with 20 µm of chromate showed no corrosion when exposed to chlorides. In contrast, uncoated aluminium has a higher corrosion potential (E_{corr}), whereas the corrosion current density (I_{corr}) decreases as the thickness of the chromate coating on aluminium increases [35-39]. The Bode plot, depicted in Figures 4a and b, demonstrates that the rise in absolute impedance at low frequencies corroborates the enhanced protection linked to the augmentation of chromic acid concentration, which peaks at 0.5 percent before declining. The results demonstrate that the corrosion rate diminished due to the development of a chromate coating and further declined with an increase in chromic acid concentration.

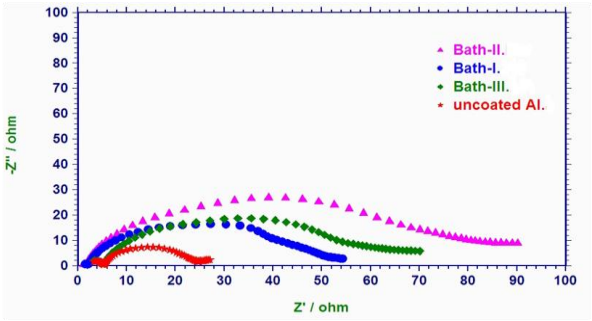


Figure 3. Comparison of Nyquist impedance plots for bare and conversion coated aluminium in solutions I, II, and III.

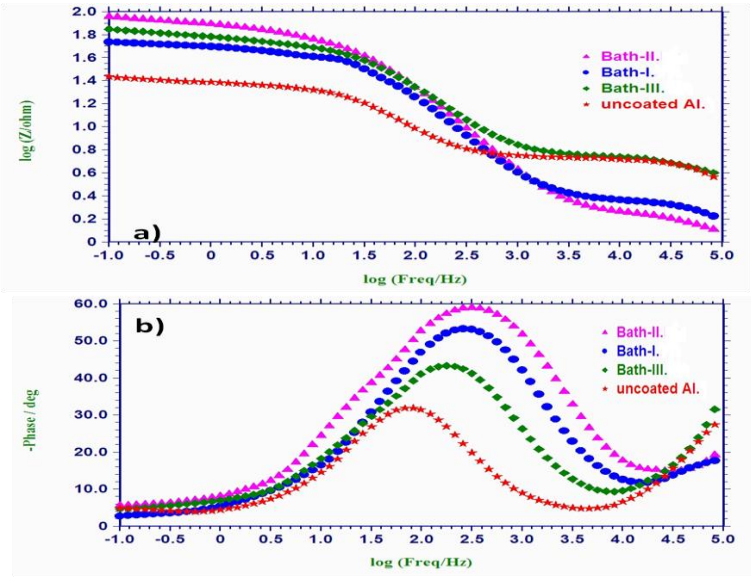


Figure 4(a, b). Bode plots for bare and chromate conversion-coated aluminium in solutions I, II, and III.

Scanning electron microscope (SEM) analysis

The surface morphology of the chromate conversion coating on aluminium was examined using scanning electron microscopy (SEM) before and after corrosion testing in a 3% NaCl solution. Figure 5 shows the SEM micrograph of the coated aluminium surface prior to exposure. The surface appears relatively uniform, with fine cracks and a somewhat porous structure typical of chromate conversion coatings. These features are indicative of a passive layer that allows limited ion transport while still offering effective corrosion resistance. The presence of microcracks may be attributed to dehydration during the drying process, but they do not significantly compromise the protective behavior due to the self-healing nature of chromate-based films. After immersion in the 3% NaCl solution for 24 hours, the SEM image reveals notable changes in surface morphology. Localized corrosion and pitting are visible in certain regions, suggesting breakdown of the coating in chloride-rich environments. However, the damage is relatively limited, implying that the coating still retains a degree of barrier protection. The comparison between pre and post exposure SEM images confirms that the chromate conversion coating offers effective initial protection against chloride-induced corrosion. However, its performance may deteriorate over time due to the penetration of aggressive chloride ions through microdefects and pores. Overall, the SEM analysis supports the electrochemical findings, indicating that the chromate coating provides short-term corrosion resistance with some susceptibility to localized attack under prolonged exposure.

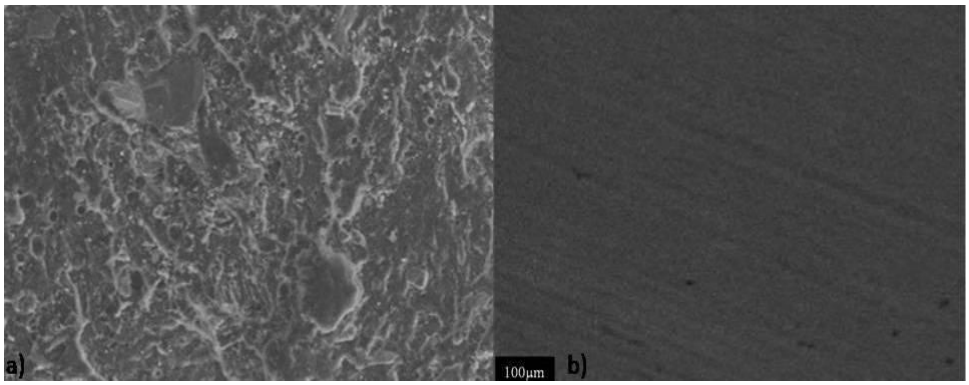


Figure 5 SEM image for a) uncoated and b) chromate-coated aluminium.

CONCLUSION

Potentiodynamic polarization, electrochemical impedance spectroscopy, and SEM analysis were used to methodically examine the electrochemical behavior of aluminum treated with chromate conversion coatings under different circumstances. The observed results clearly indicate that enhancing immersion time, temperature, and chromic acid concentration significantly improves the coating's protective properties. Conspicuously, the coating formed from solution II (0.5% of Cr_2O_3) exhibited superior corrosion resistance compared to those from solution I (0.3% of Cr_2O_3) and solution III (0.7% of Cr_2O_3). These observations are attributed to the self-healing capabilities inherent in the 0.5% of Cr_2O_3 coating. And also, when coatings from solutions I and III were applied in various environments, the corrosion resistance of aluminum treated with solution II increased, reinforcing its effectiveness. Further evaluation of porosity and adhesion confirmed the superiority of the chromate layers. SEM analysis also provided detailed insights into the surface morphology and microstructural characteristics of the coatings, well supporting the observed

electrochemical results. Overall, the 0.5% of Cr_2O_3 treatment shows optimal corrosion protection for aluminum under the experienced conditions. Further studies should investigate the long-term durability of the 0.5% Cr_2O_3 chromate conversion coating under additional diverse and harsher environmental conditions. Furthermore, researching environmentally friendly alternatives to chromate-based coatings and their comparable performance could lead to safer and more sustainable corrosion protection approaches. Advanced methodologies for characterization may also be used to better understand the self-healing mechanisms at the nanoscale.

REFERENCES

1. Oki, M.; Adediran, A.A.; Ikubanni, P.P.; Adesina, O.S.; Adeleke, A.A.; Akintola, S.A.; Edoziuno, F.; Aleem, A. Corrosion rates of green novel hybrid conversion coating on aluminium 6061. *Results Eng.* **2020**, 7, 100159.
2. Becker, M. Chromate-free chemical conversion coatings for aluminum alloys. *Corros. Rev.* **2019**, 37, 321-342.
3. Shwetha K.M.; Praveen, B.M.; Devendra, B.K. A review on corrosion inhibitors: Types, mechanisms, electrochemical analysis, corrosion rate and efficiency of corrosion inhibitors on mild steel in an acidic environment. *Results Surf. Interfaces* **2024**, 16, 100258.
4. Li, S.–S.; Yue, X.; Li, Q.–Y.; Peng, H.–L.; Dong, B.–X.; Liu, T.–S.; Yang, H.–Y.; Fan, J.; Shu, S.–L.; Qiu, F.; Jiang, Q.–C. Development and applications of aluminum alloys for aerospace industry. *J. Mater. Res. Technol.* **2023**, 27, 944-983.
5. Soufeiani, L.; Foliente, G.; Nguyen, K. T. Q.; San Nicolas, R. Corrosion protection of steel elements in façade systems – A review. *J. Build. Eng*. **2020**, 32, 101759.
6. Kumaran, T.S.; Prakasam, A.; Venkatesh, G.; Vennila, P.; Sheena, M.Y.; Parveen B.S. Design and synthesis of phenylacridine-based organic dyes and their applications in dye-sensitized solar cells. *Russ. J. Phys. Chem.* **2023**, 97, 2607-2623.
7. Zhang, Y.; Sun, Y.; Fan, X.; Liao, B.; Deng, C.; Li, S.; Wang, C.; Xv, Y.; Li, K.; Lv, Y. Corrosion behavior of WC-NiMoCrFeCo coating in seawater environment: Positive corrosion inhibition of a novel dynamic reaction product. *Chem. Eng. J.* **2025**, 507, 160568.
8. Priyantoro, D.; Mulyani, E.; Sujitno, T. Effect of nitrogen ion implantation on the surface hardness, corrosion rate, and crystal structure of pure aluminium. *Adv. Mater.* **2019**, 8, 137-141.
9. Liu, Z.; Xiao, Y.; Yang, L.; Liu, W.; Yan, G.; Sun, Y.; Zhou, Y. Failure prediction of thermal barrier coatings on turbine blades under calcium-magnesium-alumina-silicate corrosion and thermal shock. *Acta Mech. Sin.* **2025**, 41, 424285.
10. Palanisamy, S.P.; Maheswaran, G.; Selvarani, A.G.; Kamal, C.; Venkatesh, G. *Ricinus communis* – A green extract for the improvement of anti-corrosion and mechanical properties of reinforcing steel in concrete in chloride media. *J. Build. Eng.* **2018**, 19, 376-383.
11. Annaamalai, M.G.L.; Maheswaran, G.; Ramesh, N.; Kamal, C.; Venkatesh, G.; Vennila, P. Investigation of corrosion inhibition of welan gum and neem gum on reinforcing steel embedded in concrete. *Int. J. Electrochem. Sci.* **2018**, 13, 9981-9998.
12. Palanisamy, S.P.; Maheswaran, G.; Kamal, C.; Venkatesh, G. *Prosopis juliflora*—A green corrosion inhibitor for reinforced steel in concrete. *Res. Chem. Intermed.* **2016**, 42, 7823-7840.
13. Leng, B.; Xue, Y.; Li, J.; Qi, J.; Yi, A.; Zhao, Q. A critical review of anti-corrosion chemical surface treatment of aluminum alloys used for sports equipment. *Crystals* **2024**, 14, 101.
14. Zhang, H.; Zhang, X.; Zhao, X.; Tang, Y.; Zuo, Y. Preparation of Ti–Zr-based conversion coating on 5052 aluminum alloy, and its corrosion resistance and antifouling performance. *Coatings* **2018**, 8, 397.

15. Domínguez-Crespo, M.A.; Onofre-Bustamante, E.; Torres-Huerta, A.M.; Rodríguez-Gómez, F.J. Morphology and corrosion performance of chromate conversion coatings on different substrates. *J. Mex. Chem. Soc.* **2008**, 52, 235-240.
16. Hesamedini, S.; Ecke, G.; Bund, A. Structure and formation of trivalent chromium conversion coatings containing cobalt on zinc plated steel. *J. Electrochem. Soc.* **2018**, 165, 657-669.
17. Vaghefinazari, B.; Wierzbicka, E.; Visser, P.; Posner, R.; Arrabal, R.; Matykina, E.; Mohedano, M.; Blawert, C.; Zheludkevich, M.L.; Lamaka, S.V. Chromate-free corrosion protection strategies for magnesium alloys—A review: Part III—corrosion inhibitors and combining them with other protection strategies. *Materials* **2022**, 15, 8489.
18. Omari, I.; Penafiel, J.; McIndoe, J.S. Chromate conversion coating and alternatives as corrosion-resistant treatments for metal parts. *ChemRxiv* **2020**, 1, 12451208.
19. Dzhurinskiy, D.V.; Dautov, S.S.; Shornikov, P.G.; Akhatov, I.S. Surface modification of aluminum 6061-O alloy by plasma electrolytic oxidation to improve corrosion resistance properties. *Coatings* **2021**, 11, 4.
20. Di Sarli, A.R.; Culcasi, J.D.; Tomachuk, C.R.; Elsner, C.I.; Ferreira-Jr, J.M.; Costa, I.A Conversion layer based on trivalent chromium and cobalt for the corrosion protection of electrogalvanized steel. *Surf. Coat. Technol.* **2014**, 258, 426-436.
21. Oki, M.; Adediran, A.A.; Ogunsemi, B.; Agboola, O.O.; Olayinka, S.; Ogunsola, O. Improvement in corrosion resistance of aluminium alloy by permanganate-based conversion coating. *J. Phys. Sci.* **2018**, 29, 13-24.
22. Munson, C.A.; McFall-Boegeman, S.; Swain, G.M. Cross comparison of TCP conversion coating performance on aluminum alloys during neutral salt-spray and thin-layer mist accelerated degradation testing. *Electrochim. Acta* **2018**, 282, 171-184.
23. Murugaiyan, M.; Madhu, P.; Vennila, P.; Venkatesh, G. Investigation of Schiff base N,N'-bis(salicylidene-1,2-diaminoethane) (salen) as corrosion inhibitor for mild steel in H_3PO_4 solution. *Int. J. Chem. Tech. Res.* **2015**, 7, 2489-2498.
24. Hamdy, A. S.; Hussien, H. M. The effect of solution pH of permanganate coating on the electrochemical characteristics of ZE41 magnesium alloy in chloride media. *Int. J. Electrochem. Sci.* **2014**, 9, 2682-2695.
25. Gao, Z.M.; Han, X.B.; Dang, L.H.; Wang, Y.; Bi, H.C. Evaluation of simulated atmospheric corrosion of Q235 steel by wavelet packet image analysis. *Int. J. Electrochem. Sci.* **2012**, 7, 9202-9212.
26. Ofoegbu, S.U.; Fernandes, F.A.O.; Pereira, A.B. The sealing step in aluminum anodizing: A focus on sustainable strategies for enhancing both energy efficiency and corrosion resistance. *Coatings* **2020**, 10, 226.
27. Shim, B.Y.; Kim, H.; Han, C.N.; Jang, Y.B.; Yun, J.W. Characteristics of Cr(III)-based conversion coating solution to apply aluminum alloys for improving anti-corrosion properties. *J. Microelectron. Packag. Soc.* **2016**, 23, 79-85.
28. Vennila, P.; Kavitha S.; Venkatesh, P.Madhu, P. Experimental and theoretical investigation of Rosmarinus officinalis leaves extracts as the corrosion inhibitor for mild steel in H_3PO_4 solution; Synergistic effect. *Der Pharma Chemica*. **2015**, 7 275-283.
29. Asadi, V.; Danaee, I.; Eskandari, H.; Nikmanesh, S. Electrochemical studies on corrosion resistance of phosphate chemical conversion coatings on low carbon steel API 5L grade B, *Songklanakarin. J. Sci. Technol.* **2018**, 40, 147-153.
30. Abrashov, A.; Grigoryan, N.; Vagramyan T.; Asnis N. On the mechanism of formation of conversion titanium-containing coatings. *Coatings* **2020**, 10, 1-11.
31. Edoziuno, F.O.; Adediran, A.A.; Odoni, B.U.; Nwaeju, C.C.; Adesina, O.S.; Oki, M. Influence of wormin mebendazole on the corrosion of mild steel in 1.0 M sulphuric acid. *Results Eng.* **2021**, 9, 100192.

32. Zhu, W.; Chen, F.; Yi, A.; Liao, Z.; Li, W.; Li, K.; Chen, K.; Liang, G.; Guo T.J.; Wu, Q. Titanium, zirconium and vanadium conversion coatings (TZVCCs) on AZ91D magnesium alloy sheets, *Mater. Res. Express* **2020**, 7, 086402.
33. Aliofkhazraei, M.; Walsh, F. C.; Zangari, G.; Köçkar, H.; Alper, M.; Rizal, C.; Magagnin, L.; Protsenko, V.; Arunachalam, R.; Rezvanian, A.; Moein, A.; Assareh, S.; Allahyarzadeh, M. H. Development of electrodeposited multilayer coatings: a review of fabrication, microstructure, properties and applications. *Appl. Surf. Sci. Adv.* **2021**, 6, 100141.
34. Duan, G.; Yang, L.; Liao, S.; Zhang, C.; Lu, X.; Yang, Y.; Zhang, B.; Wei, Y.; Zhang, T.; Yua, B.; Zhange, X.; Wangc, F. Designing for the chemical conversion coating with high corrosion resistance and low electrical contact resistance on AZ91D magnesium alloy. *Corros. Sci.* **2018**, 135, 197-206.
35. Bahram, V.; Sviatlana V.L.; Eugen, G.; Kiryl, Y.; Carsten, B.; Maria, S.; Nico, S.; Florian, W.D.C.; Mikhail, L.Z. Corrosion inhibition of decylphosphonate on bare and PEO-coated Mg alloy. *Corros. Sci.* **2024**, 226, 111651.
36. Jin, S.; Ma, X.; Wu, R.; Tingqu, Li.; Jiaxiu Wang, Boris L.; Krit, Hou, L.; Zhang, J; Wang, G. Effect of carbonate additive on the microstructure and corrosion resistance of plasma electrolytic oxidation coating on Mg-9Li-3Al alloy. *Int J Miner Metall Mater*. **2022**, 29, 1453-1463.
37. Venkatesh, G.; Kamal, C.; Vennila, P.; Kaya, S.; Annaamalai, M.G.L.; Ibrahimi, B.L. Sustainable corrosion inhibitor for steel embedded in concrete by Guar Gum: Electrochemical and theoretical analyses. *Appl. Surf. Sci*. **2022**, 12, 100328.
38. Hallemans, N.; Howey, D.; Battistel, A.; Saniee, N. F.; Scarpioni, F.; Wouters, B.; La Mantia, F.; Hubin, A.; Widanage, W. D.; Lataire, J. Electrochemical impedance spectroscopy beyond linearity and stationarity: A critical review. *Electrochim. Acta* **2023**, 466, 142939.
39. Byeon, H.; Haribabu, K.; Kiradoo, G.; Sreenivasan, V. S.; Sivaprakash, M.; Richard, S.; Sunil, J. Evaluation of physiochemical and electrochemical behaviour of reduced graphene functionalized copper nanostructure as an effective corrosion inhibitor. *Bull. Chem. Soc. Ethiop*. **2024**, 38, 269-280.